



OPEN

# Wireless control and selection of forces and torques - towards wireless engines

SUBJECT AREAS:

ELECTRICAL AND  
ELECTRONIC  
ENGINEERINGACTUATORS  
METAMATERIALS  
APPLIED PHYSICS

M. Boyvat, C. Hafner &amp; J. Leuthold

Institute of Electromagnetic Fields (IEF), ETH Zurich, Switzerland.

Received  
24 March 2014Accepted  
19 June 2014Published  
18 July 2014Correspondence and  
requests for materials  
should be addressed to  
M.B. (mboyvat@ethz.  
ch)

**Powering and manipulating translational and rotational motions of objects wirelessly, and controlling several objects independently is of significant importance in numerous fields such as robotics, medicine, biology, fluid dynamics, optics. We propose a method based on coupled LC resonators, to control objects selectively by steering the frequency of an external magnetic field. This concept does not need any magnetic materials and it brings a rich variety of features concerning forces and torques. We theoretically and experimentally show that the forces can be enhanced by the interaction of resonators and that both direction and magnitude of forces can be controlled by the frequency of the applied external magnetic field. Moreover, we demonstrate interesting rotational effects, such as bi-directionally controllable torques, controllable stable orientations, and spinning, which leads to a wirelessly powered motor.**

The mechanical effects acting on adjacent rings carrying current have attracted the interest of the community a while ago, see e.g. Kim et al.<sup>1</sup>. However, new phenomena are expected if these simple conductive rings are converted to resonant structures by adding capacitors. In fact, coupled resonator structures, e.g., coupled pendulums in mechanics, tend to exhibit highly complex behavior, which may also be observed for coupled resonators studied in the following. Resonances play an extraordinary role in physics because they offer strong responses to weak signals. The simplest electrical resonators are obtained from inductances (L) and capacitances (C). Such LC resonators are based on the exchange of electric and magnetic energy. They have a long history and were extensively used already in the 19<sup>th</sup> century<sup>2</sup>. Despite of this, they have not stopped opening new routes in research. In 2000, electromagnetic metamaterials, which provide naturally inaccessible electromagnetic properties, were introduced and attracted enormous scientific attention<sup>3–8</sup>. These man-made materials are composed of so-called meta atoms and resonances due to inductive and capacitive parts in the meta atoms are responsible for their interesting electromagnetic properties. In 2007 efficient resonant wireless energy transmission was demonstrated, where electric resonators have taken an important role again<sup>9</sup>.

The enhancement of forces due to resonances has led to remarkable progress in mechanical effects in the optical domain<sup>10–13</sup> and, the mechanical influences on metamaterials and meta-atoms are attention grabbing topics in the metamaterial community<sup>14–21</sup>.

In this paper, we will exploit the enhancements of electromagnetic resonances to independently exert magnetic forces on different remote objects. We show that both translational and rotational forces can be induced if the objects have different resonance frequencies of a sufficiently high quality factor. In particular we will discuss and demonstrate (1) how magnetic induction can power and control the translational forces and (a) induce both attractive and repulsive forces and (b) how these forces may be steered by the frequency of the external field. (2) We will further demonstrate how rotational forces, i.e. torques can be induced remotely by detuning the external magnetic field frequency. More precisely, (a) we will show how the torque on an LC resonator can be controlled bi-directionally by the frequency. (b) We then show, how a stable orientation of the angle of an LC resonator in an external magnetic field may be changed by the frequency and (c) we demonstrate how interacting resonators can be used to induce continuous rotations – i.e. used to power a “wireless motor”.

Powering and controlling force or motion agents with advanced mechanical effects in an untethered way is highly interesting for many applications, e.g., 1) the control of micro scale robots and actuators<sup>22–29</sup>, especially manipulating several of them independently<sup>30–37</sup>, and 2) applications where shape control is desired, for instance in adaptive optics<sup>38–40</sup> and tunable metamaterials<sup>16,41,42</sup>. Rotational features may also be helpful in microvalves<sup>43</sup>, microstirrers<sup>44,45</sup>, and orientation-free wireless charging of wireless robotic endoscopic capsules<sup>46–49</sup>.

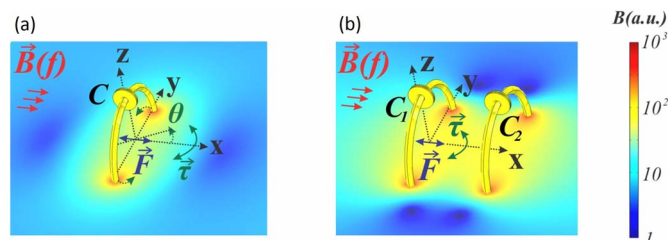


**Figure 1** | LC resonators in an external magnetic field sense magnetically induced mechanical effects, i.e., translational forces ( $F$ ) or torques ( $\tau$ ). The color shows the magnitude of magnetic flux density  $B$ . (a), Single resonator. (b), Two coupled resonators. The interaction of resonators is helpful for obtaining enhanced and more advanced mechanical effects.

## Theory and calculations

**Single resonator.** We first discuss the forces exerted by a magnetic field onto a single resonator comprising of a conductive loop with a capacitor  $C$ , see Fig. 1a.

When a conductive single loop is placed in a time varying magnetic field, a current is induced in the loop according to Faraday's law, which also leads to Lorentz forces acting on the currents. If the loop is connected to a capacitor, the current and the forces can be enhanced significantly near the resonance frequency. The resonance frequency of an ideal LC resonator is given by  $f_0 = 1/(2\pi\sqrt{LC})$ , where  $L$  is the inductance of the coil and  $C$  is the capacitance in the resonator. In practice, the magnitude of the current at resonance is limited by an inevitable resistance  $R$ , which is mostly due to Ohmic loss in the conductors.

When a magnetic field and a current loop interact, Lorentz forces act on the current loop. If the magnetic field is time harmonic, the Lorentz force has AC and DC parts. When the frequency of the current is sufficiently high, the AC part of the force is negligible and only the static DC force is relevant. In a homogenous magnetic field  $\vec{B}$  there are no net translational forces and only when the magnetic field has a gradient, the resonator senses a net force<sup>50</sup>. Its magnitude and direction can be steered by the frequency of the external field. It is important to note that the force exerts in different directions below and above resonance, and that the magnitude can be changed both by the strength of the external field and by the frequency. If the gradient of the magnetic field is small, the forces are small and they vanish in a uniform magnetic field. As shown in the following section, using pairs of resonators removes the problems of having a substantial gradient<sup>33</sup>.

Interestingly, the LC resonator senses a torque even in a uniform magnetic field and the torque acting on LC resonators as the building unit of metamaterials has already led to several interesting results<sup>17,19,21</sup>. The torque can be calculated from the formula for a magnetic dipole moment:

$$\tau_z = A \cdot I_{RMS}(f, f_0) \cdot B_{RMS}(f) \cos(\Delta\varphi(f, f_0)) \sin(\theta), \quad (1)$$

where the  $z$ -axis is chosen to be the axis of the rotation (see Fig. 1a).  $A$  is the effective area of the current loop.  $B_{RMS}$  is the RMS magnetic flux density.  $\Delta\varphi$  is the phase difference between the applied magnetic flux density and the current induced on the resonator.  $\theta$  is the angle between the direction of the magnetic flux density and the axis of the resonator ( $\theta$  is zero when the resonator lies in the  $yz$  plane as in Fig. 1a).

From equation (1) we see that the resonator senses a torque around the  $z$ -axis if its axis is neither parallel (i.e.  $\sin(\theta)$  is zero) nor perpendicular ( $I_{RMS}$  is zero) to the magnetic flux density. Similar to the forces, the direction of rotation can change for frequencies below and above resonance. The magnitude can be influenced by changing the frequency or the magnitude of the external field. Moreover, there are stable positions of the resonator, which

change for frequencies below and above resonance. The resonator is in stable equilibrium below resonance when the direction of its axis is parallel to the magnetic flux density, whereas it is stable above resonance when its axis is perpendicular to the magnetic flux density. Both the force and the torque increase quadratically with increasing  $B$ , because the current in the resonator is linearly proportional to  $B$ .

**Translational forces in multiple resonators. Axial bidirectional forces in coupled resonators.** Studying a single resonator is a first step to understand the behavior of a system of resonators, but what can be done by a single resonator is very limited and well known. Coupled resonators exhibit a rich variety of effects that usually may not be easily understood. Therefore, engineering of configurations of coupled resonators is demanding and must be done by appropriate simulations. This is probably the main reason why not much work has been presented on systems of coupled LC resonators.

The simplest system of resonators is a pair of resonators. When two identical LC resonators are magnetically coupled with a mutual inductance  $M$ , resonance splitting happens, i.e., instead of a single resonance frequency, two resonance frequencies are obtained.

Near resonance, the magnetic field energy is concentrated in a small area around the coils as illustrated in Fig. 1. This enhances the magnetically induced mechanical effects on the resonators significantly. In a hypothetical, loss-free resonator, the currents and therefore the forces would even go to infinity. In practice, the inevitable resistance  $R$  reduces the quality factor of the resonator and limits currents and forces.

For an axial arrangement as shown in Fig. 1b, the mutual inductance  $M$  is positive<sup>51</sup> and the currents in the two resonators are in phase at the lower resonance frequency  $f_1$ . Consequently, the resonators attract each other. At the higher resonance frequency  $f_2$ , currents have opposite phases. This causes repulsion. However, because of the anti-symmetry of the higher resonance, it is almost not excited and this repulsion could not be observed experimentally. A method to excite the higher resonance is using two resonators with different resonance frequencies. This can be realized by simply changing one of the capacitances. The corresponding calculations are shown in Fig. 2. It is important to note that cheap inductors (coils with many turns) were used for the experiments. Simulations of these coils would lead to very high computational costs. In order to reduce the computational effort, much simpler inductors with single turn loops were considered for the calculations. In order to obtain results comparable to the measurements, 2.5 cm loop radii were used and the self-inductance of the loop was set to 0.15  $\mu\text{H}$  by choosing a proper wire diameter<sup>52</sup>. This choice guarantees that the ratios of self-inductance and mutual inductance values of the calculations are similar to those in the experiments. For the calculations, the capacitances connected to the conductive loops are equal and 400 pF in the case of identical resonators and 400 pF and 600 pF in the case of different resonators. The corresponding values in the experiments were 1 mH inductance, 1  $\mu\text{F}$  and 1.5  $\mu\text{F}$  capacitances: As a consequence, resonance frequencies in calculations are higher by the factor 4082. Furthermore, the quality factors of the resonators in simulations were set to 30, so that the quality factors of the resonators in simulations and measurements are similar. The influence of the quality factor is shown in Supplementary Fig. 2.

**Lateral forces in coupled resonators and selectively activated trapping points.** Lateral forces on the resonators also show interesting properties. When the axis of two resonators with circular current loops are aligned, there is no lateral force because the contributions of both the external magnetic field and the induced magnetic field exert forces that both vanish due to symmetry. However, any lateral offset causes lateral forces as already calculated in a detailed way in an earlier work for current loops without capacitors<sup>1</sup>. With capacitors, the direction and the magnitude of the forces can be changed by the

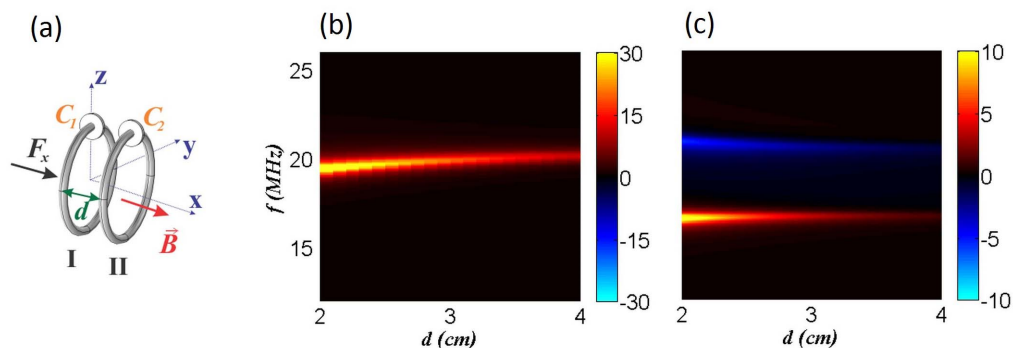
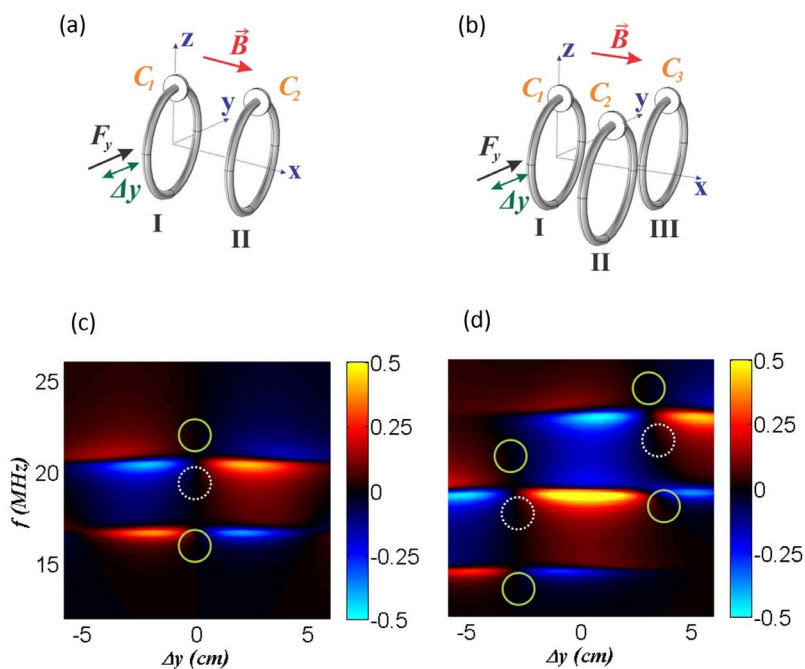


**Figure 2 | Axial forces in a pair of resonators.** (a), Schematic of the resonators.  $\vec{B}$  is the external magnetic field density.  $d$  is the distance between the resonators.  $C_1$  and  $C_2$  are the capacitances in the resonators, and  $F_x$  is the axial force on the first resonator. (b), Attractive forces as obtained by two identical resonators. The plot shows the axial force  $F_x$  on the first resonator depending on frequency  $f$  and distance  $d$ . The color corresponds to the force in arbitrary units. Only attractive forces are obtained. The resonance frequency shift towards lower frequencies is larger when the distance between resonators is smaller. (c), Attractive (red-yellow area) and repulsive (blue) forces are obtained for resonators with two different capacitors.  $F_x$  depends on the frequency  $f$  and distance  $d$  for different resonators. Both attractive (red-yellow area) and repulsive (blue) forces can now be obtained.

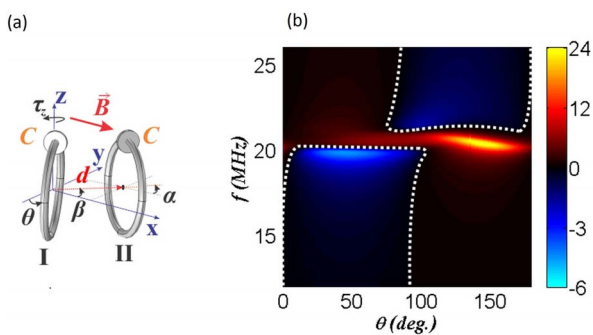
frequency – similar to what has been observed for the axial forces. More interestingly, the lower resonance offers a trapping point in the  $yz$  plane, see the points marked by a circle in Fig. 3a and Fig. 3c. The resonator senses a restoring force which tries to pull the resonator back to the trapping point independent of the lateral offset. By only changing the frequency, the trapping point can be converted to a repulsive point at which any lateral displacement causes the resonator to move away. Fig. 3c shows the change of the force in  $y$  direction with respect to the displacement in  $y$  direction. The same is valid for displacements in any lateral direction (i.e. any direction in the  $y$ - $z$ -plane) because of the symmetry of the configuration.

Fig. 3b and Fig. 3d illustrate the trapping for a system with three resonators. If two of the resonators are at fixed positions in space, the trapping point for the other resonator is given. The trapping position can be switched by the frequency of the external field. This demonstrates that multiple trapping points can be formed in space. Each trapping point is activated by an appropriate frequency of the external field.

**Rotational forces and motor.** An interesting outcome of the mechanical properties of the LC resonators is a new type of wirelessly powered ‘motor’, which can operate in a uniform magnetic field and



**Figure 3 | Lateral forces in coupled resonator systems with respect to frequency and lateral displacement.** (a), Schematic of a pair of resonators with different capacities.  $\Delta y$  is the displacement of the first resonator in  $y$  direction whereas the second resonator is kept fixed.  $\vec{B}$  is the external magnetic field density.  $C_1$  and  $C_2$  are the capacitances of the resonators, and  $F_y$  is the force in  $y$  direction on the first resonator. (b), Schematic of three resonators. The first resonator is able to move whereas the other ones are fixed. (c),  $F_y$  as a function of frequency and displacement  $\Delta y$  for a pair of resonators. The color corresponds to the force in arbitrary units. At frequencies below the lower resonance and above the higher resonance, the first resonator is trapped at a stable equilibrium position (shown by the green continuous circles). When detuning the frequencies an unstable point (shown by the white dotted circle) is obtained, where any displacement causes the first resonator to diverge from its equilibrium position. (d),  $F_y$  of the first resonator as a function of frequency and displacement  $\Delta y$  for a three resonator system. Several stable and unstable trapping points can be obtained. Switching between them can be done by changing the frequency of the external field.



**Figure 4 | Exerting a continuous rotation in a resonator system.** (a), The schematic shows the arrangement for inducing a continuous rotation onto resonator I. It is assumed that the resonator I is free to rotate around the  $z$  axis. Resonator II is fixed and placed off-axis at a distance  $d$  and angle  $\beta$ , twisted by the angle  $\alpha$  with respect to  $x$ -axis. For the simulations,  $d = 4$  cm and  $\beta = \alpha = 45^\circ$  with respect to the  $x$  axis was assumed for the resonator II.  $\theta$  is the rotation angle of the first resonator. (b), Torque with respect to frequency and rotation angle  $\theta$ . The color shows the  $z$  component of the torque,  $\tau_z$ . One can see that the torque  $\tau_z$  has dominant and strong contributions in a certain frequency range. The borders between positive and negative torques are shown by white dotted lines.

does not need any external rotating magnetic fields, any contacts or any magnetic materials.

The simplest approach for constructing such a motor is to place a single resonator in an externally generated magnetic field. When the external field has a single frequency, the resonator is stabilized along one of its stable orientations as discussed above in the single resonator case. By modulating the frequency of the external magnetic field, one can provide torque for a continuous rotation around the  $z$ -axis. However, this requires synchronization of the external field with the actual angular rotation velocity and the orientation of the coil. Without synchronization, a rather chaotic motion would be observed.

A scheme with two resonators will allow one to induce rotational forces for a continuous rotation without the need for synchronization. Fig. 4a shows two identical ring resonators that are placed close to each other. The first one may rotate around the  $z$  axis, while the second one is fixed in an off-axis position at a distance  $d$  and an angle  $\beta$ , twisted by an angle  $\alpha$ . The torque exerted on the first coil as a function of the angular position  $\theta$  and of the frequency of the external field for this arrangement is plotted in Fig. 4b. It can be seen that there is a frequency band within which the torque is always positive independent of the angular position of the first coil. This means that one can exert a continuous rotation onto a coil – which is nothing else but a very simple, wirelessly powered ‘motor’. This motor consists of two identical LC resonators, a rotating one and a fixed one. The scheme does not require any frequency modulation or synchronization and it operates even in a uniform magnetic field without any contact to the two resonators. To check the sensitivity of the behavior to the non-uniformity of the external field  $\vec{B}$ , calculations were repeated with a source coil with a 5 cm radius (not shown in the picture) and the resonator coils shown in Fig. 4a. The resonator configuration was offset by  $x = 3$  cm from the center of the source coil. As a result, the external field magnitude at the center of the second resonator coil was less than half of that at the center of the first resonator. While this affects the magnitude of the torque, the characteristic of the torque is almost the same even in such a non-uniform external field.

## Experiments

Experiments proving the basic concepts of frequency controlled remote forces and torques have been performed with larger objects

and at very low frequencies. Fig. 5a depicts the experimental setup. The resonators are made of commercially available coils and capacitors. “ $d$ ” is the separation distance between resonators. The external magnetic field is produced by a larger coil. The use of lumped capacitors and coils to confirm the simulations is a valid path for lower frequencies. At very high frequencies, such as optical frequencies, one needs to resort to nano-scale fabrication processes. Moreover, at higher frequencies a force calculation requires the consideration of electrical charges.

Figure 5b shows the frequency dependence of the attractive force for three different distances. The dashed lines represent measured curves. The solid lines are derived from calculations as outlined in the ‘Methods’ section. When a second resonator is placed close to the first resonator, the forces are enhanced significantly, as one may clearly see in Fig. 5b when comparing the single resonator case with the coupled resonator cases. When the distance is increased, the mutual coupling and the resonance frequency shift decrease. Moreover, the attractive force between the resonators decreases with increasing separation distance. Note that the resonators used in the experiments are quite lossy because rather cheap coils with thin wires were used. As a result, the quality factors of the resonators are only around 30. At higher frequencies, one can obtain much higher quality factors, thus resonance effects could be much more pronounced.

In Figure 5c, the experimental (dashed) and analytical (solid) plots show that not only unidirectional forces but also bidirectional forces can be produced. This proves that not only the strength of the force but also its direction may be changed by the frequency of the external field. For the case of identical resonators in Fig. 5b, the second resonance is almost not excited and we do not see any repulsive forces as expected from theory. Fig. 5c shows that a repulsive force emerges when using two different resonators with different resonance frequencies (i.e. with different capacitors).

Figure 5d shows that the force depends quadratically on the magnitude of the external field as expected from theory. The measured forces in the experiment are in the order of several tens of mN for external magnetic flux densities in the order of 1 mT RMS.

All of the plots in Fig. 5 and further below have been performed with the same setup, details of which are given in ‘Methods’ section. The inductance of the coils is 1 mH. For the case of identical resonators, both capacitances are 1  $\mu$ F, whereas for the case of different resonators one of the capacitances is changed to 1.5  $\mu$ F. The calculated resonance frequencies of the resonators with 1 and 1.5  $\mu$ F are 5033 Hz and 4109 Hz, respectively. The resonator resistance measured around the operating frequencies is approximately  $R = 1 \Omega$ . For the calculations we used the inductance and capacitance values provided by the vendor. For the mutual inductance and resistance, the measured values of the mutual inductance ( $M = 0.16$  mH at  $d = 0.75$  cm, 0.077 mH at  $d = 1.75$  cm and 0.043 mH at 2.75 cm) and resistance ( $R = 1 \Omega$ ) were used. The frequency shift between the calculated and experimental curves is mainly attributed to the tolerances of the inductors and capacitors used in the experiments and the measurement errors in mutual inductances. More details about the calculations are given in the ‘Methods’ section.

It is very instructive to also discuss the options for inducing torques by a single resonator. The torque exerted on an LC resonator placed in a time-harmonic external magnetic field is shown in Fig. 6a. The response depends on the relative position of the ring with respect to the external magnetic field and is described by the angle  $\theta$ . If the resonator is neither parallel nor perpendicular to the external field, i.e. if  $\theta \neq 0^\circ$  and  $\theta \neq 90^\circ$  then the strength and direction of the torque depend on the frequency as shown in Fig. 6a. Furthermore, if the ring is aligned in parallel or perpendicular to the external field, the torque vanishes and a stable equilibrium position is reached if the external field is oscillating at a frequency below the resonance frequency, or if the external field is oscillating at a frequency above the resonance

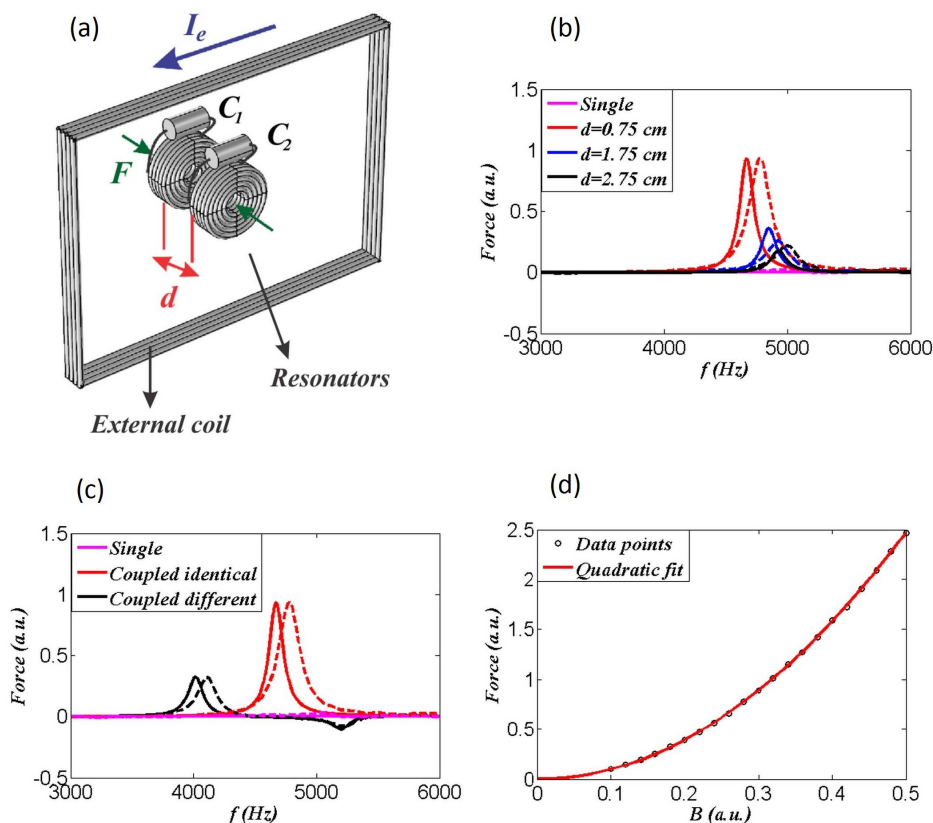


**Figure 5 | Force enhancement and bidirectional forces in a coupled resonator system.** (a), Schematic of the experimental setup. Single or coupled resonators made of coils and capacitors are excited by a larger coil (external coil) carrying a current  $I_e$ .  $F$  shows the force acting on the resonators.  $d$  is the separation distance between the resonators. (b), Frequency dependence of measured (dashed lines) and calculated (continuous lines) forces for the cases of a single resonator (pink color) and a system of identical resonators (black, blue and red colors). The forces exerted in a system with identical resonators increase with decreasing distances between the resonators and are way larger than the forces in a single resonator. (c), Bidirectional forces can be observed if the coils have different resonances (black plots). To compare the relative strengths we also have plotted the forces exerted onto coupled rings with identical resonances and a single ring. The distance between the rings is 0.75 cm. (d), Experimental verification of the quadratic dependence of the force on the magnitude of the external magnetic field.

frequency, respectively, as can be seen in Fig. 6b,c. Any disturbance would cause a compensating torque, which is different below and above resonance as illustrated in Fig. 6b,c. The stable equilibrium below/above resonance is such that the magnetic flux through the resonating loop is maximized/minimized, (see supplementary movie-1 and supplementary Fig. 2 demonstrating rotational effects experimentally). This means that one can change the angular orientation of the coil by changing the frequency of the external field. With a modulated external signal, a continuous rotational motion can be obtained. Placing another resonator in the neighborhood of the resonator in a way that breaks the symmetry also can produce a continuous rotation, even with a single frequency excitation as shown in the previous section. The experimental demonstration can be seen in the supplementary movie-2. In this proof of concept demonstration we have not optimized the setup for power efficiency. We only took cheap coils from the shelf and we estimate that the resulting efficiency is rather low, i.e., of order 1%. Note the efficiency depends much on the distance between the rotating and the fixed coils. In our experiment, the distance is rather big because of the inappropriate shape of the coils. In order to minimize this distance, it is clear that the rotating coil should have the shape of a circular cylinder, which could easily be achieved, e.g., by mounting it on an appropriately shaped core. The proper design of the fixed coil is not that obvious but we are convinced that some optimization will lead to reasonably high efficiencies considerably above 10%.

## Discussion

We have proposed a wirelessly powered and controlled multiple force/motion system using LC resonators. We theoretically and experimentally have shown that LC resonators offer many interesting mechanical effects, which can be steered by the frequency of the external magnetic field. Magnetic materials are not required but combinations of LC resonators with magnetic materials are certainly possible and might help increasing the efficiency. The translational and rotational mechanical effects offer numerous opportunities, especially when systems of resonators operating at different frequency bands are employed.

Wirelessly powered and controlled bidirectional translational and rotational motions are promising for micro robots and actuators<sup>22–29</sup>. Simultaneous operation of many of them is very attractive and the selectivity offered by the proposed method may replace or enhance the current addressing methods<sup>30–37</sup>.

Having multiple force spots enables wireless shape tuning of an elastic material by applying independently controllable forces at several points. One of the potential applications of wireless shape control is the control of inhomogeneity in metamaterials, which is crucial in many fancy applications such as cloaking<sup>6</sup>. Shape control is not only important for metamaterials. For example, in adaptive optics, by using flexible materials and applying forces on them at several points, it is possible to change the shape of a mirror<sup>38–40</sup>. Embedding wirelessly powered and controlled force

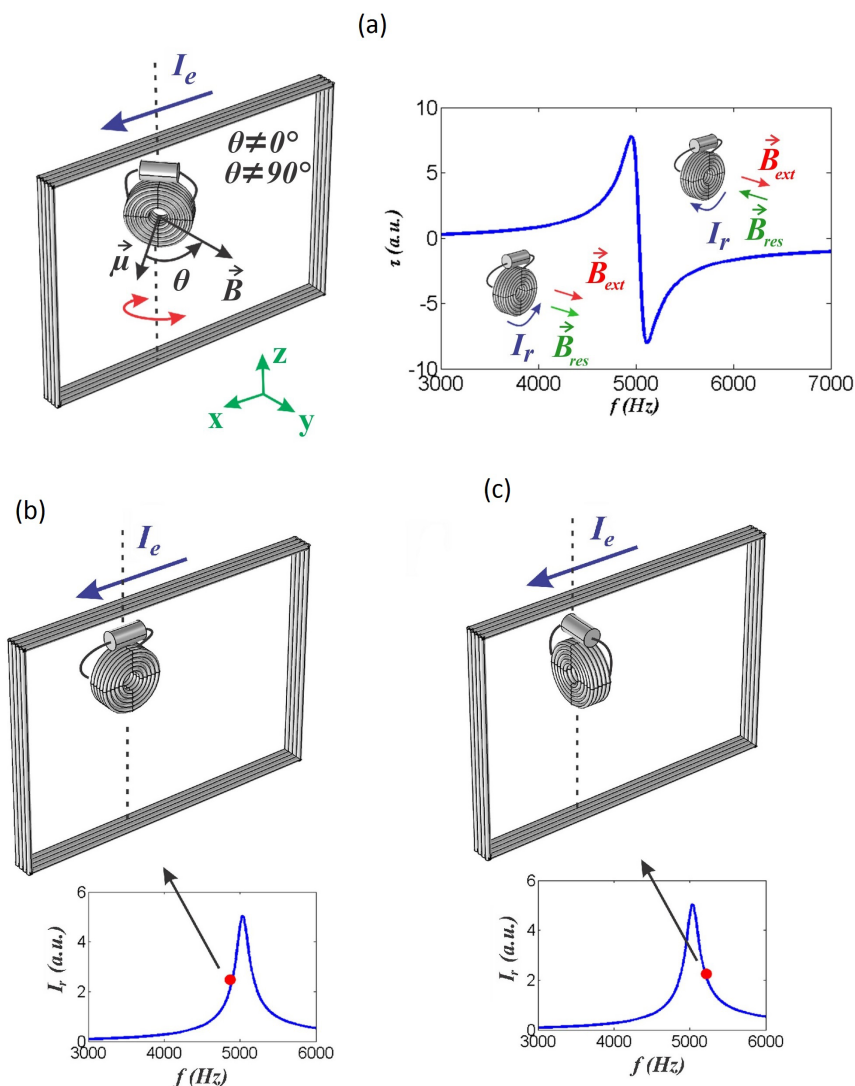


**Figure 6 | Rotational effects on an LC resonator.** (a), The schematic of the experimental setup and calculated torque.  $\mu$  is the magnetic dipole moment and  $\vec{B}$  is the magnetic flux density. Due to the sudden phase change in the current at resonance frequency, the resonator feels opposite torques below and above resonance (See supplementary movie 1 for experimental demonstration). Above resonance, the current in the resonator  $I_r$  produces a magnetic field  $\vec{B}_{res}$  opposite to the exciting field  $\vec{B}_{ext}$ , while it supports a field in the same direction as the exciting field below resonance. (b), Stable equilibrium of the resonator below resonance. The axis of the coil is parallel to the exciting field. (c), Stable equilibrium of the resonator above resonance. The axis of the coil is perpendicular to the exciting field.

actuators which are made of resonators would remove the tethering necessity.

The rotational features may also contribute to many other applications. Typical examples are microvalves<sup>43</sup>, microstirrers<sup>44,45</sup>, and orientation adjustment of wireless power transfer coils in applications where the device to be charged does not have a fixed orientation, e.g., wireless robotic endoscopic capsules<sup>46–49</sup>.

## Methods

**Theoretical calculations.** The static force  $\vec{F}$  on the resonator depends on the geometry of the loop, the magnitudes of the field and of the current, and the phase difference  $\Delta\phi$  between field and current

$$\vec{F} = \int I_{RMS}(f, f_0) \vec{dl} \times \vec{B}_{RMS}(f) \cos(\Delta\phi(f, f_0)). \quad (2)$$

Here,  $I_{RMS}$  and  $B_{RMS}$  are RMS values of the current and the magnetic flux density. The integration is performed over a path along the current loop.

The torque is calculated similarly

$$\vec{\tau} = \int \vec{r} \times (I_{RMS}(f, f_0) \vec{dl} \times \vec{B}_{RMS}(f)) \cos(\Delta\phi(f, f_0)), \quad (3)$$

where  $\vec{r}$  is the displacement vector from the point around which the torque is calculated. The current and its phase are found by

$$\mathcal{I} = \frac{-j\omega \cdot \iint \vec{B} \cdot \vec{dA}}{j\omega L + 1/(j\omega C) + R}, \quad (4)$$

where  $\omega = 2\pi f$ ,  $\mathcal{I}$  and  $B$  are complex current and complex magnetic flux density phasors<sup>53</sup>. The integration is performed over the surface of the coil  $A$  to find the magnetic flux through the coil.

Resonance frequencies of a coupled resonator system are given by the following equations:

$$f_1 = \frac{1}{2\pi\sqrt{(L+M)C}} \text{ and } f_2 = \frac{1}{2\pi\sqrt{(L-M)C}}. \quad (5)$$

For the theoretical calculations shown in Fig. 2, 3 and 4, a large external circular current loop with 30 cm radius is placed in the  $yz$  plane as a magnetic field source whereas the resonators have 2.5 cm radius and are placed at the center of the outer loop. All resonators have a single turn in order to minimize the computational costs. The self-inductance of the resonator loops is set to 0.15  $\mu\text{H}$  by a proper selection of the wire diameter<sup>52</sup>. The wire diameter is selected in such a way that the ratios between the mutual inductances and self-inductances in theoretical calculations and in the experiments are similar. In Fig. 2,3 and 4, it is assumed that resonators have the same



quality factor  $Q = 30$  (which is the order of the quality factor of the resonators used in our experiments). From this the corresponding resistances are calculated to be  $R = 0.646 \Omega$  for  $C = 400 \text{ pF}$ ,  $R = 0.527 \Omega$  for  $C = 600 \text{ pF}$ ,  $R = 0.59 \Omega$  for  $C = 480 \text{ pF}$ ,  $R = 0.722 \Omega$  for  $C = 320 \text{ pF}$ ,  $R = 0.456 \Omega$  for  $C = 800 \text{ pF}$ . The resonance frequencies are 20.55 MHz, 16.78 MHz, 18.76 MHz, 22.98 MHz and 14.53 MHz, respectively. The magnetic field intensity produced by a circular loop is calculated analytically<sup>54</sup> and currents are calculated by equation (4). If there are multiple resonators, equation (4) is written with the effect of mutual inductances and the resulting system of equations is solved<sup>51</sup>. Forces and torques are calculated by equations (2) and (3) after finding the induced currents in the system.

**Experiments.** The external magnetic field source is a coil with multiple turns and approximately  $27 \text{ cm} \times 20 \text{ cm}$  size. The current through the external coil  $I_e$  was in the order of several A (amps) RMS to obtain magnetic flux densities in the order of 1 mT RMS. The coils used in resonators are multiple turn air-core coils with 48 mm diameter, 18 mm height, 0.85 mm wire diameter and the coil inductance value provided by the manufacturer is  $L = 1 \text{ mH}$ . The capacitance values provided by the manufacturers are 1 and  $1.5 \mu\text{F}$ .

The calculated relative forces in Fig. 5 are found by the formula relating the force to the currents and the gradient of the mutual inductance<sup>50</sup>:

$$\vec{F} = I_1 \cdot I_2 \cdot \nabla M \rightarrow F_x = I_1 \cdot I_2 \cdot \frac{\partial M}{\partial d} \quad (6)$$

The frequency characteristic of currents in a uniform magnetic field is calculated from equation (4) with the effect of mutual inductance and solving the resulting system of equations for the inductance, capacitance, resistance and mutual inductance values which are given in the 'Experiments' section<sup>51</sup>. The mutual inductance as a function of the distance was obtained experimentally and the derivative of mutual inductance with respect to the distance in equation (6) was calculated from these measurement data. In the end, the calculated forces are normalized, so that the maximum force in the measurement for identical resonators with  $d = 0.75 \text{ cm}$  and the maximum calculated force for identical resonators with  $d = 0.75 \text{ cm}$  are equal.

To measure the forces, two force sensors are placed between the resonators. One of the resonators is fixed while the other one hangs on a long thin rope. For single resonator measurements the fixed resonator is removed. The current through the external magnetic field source is monitored continuously during force measurements and the variation of the current is compensated using the quadratic dependence of forces on the external magnetic field strength.

1. Kim, K.-B., Levi, E., Zabar, Z. & Birenbaum, L. Restoring force between two noncoaxial circular coils. *IEEE Trans. Magn.* **32**, 478–484 (1996).
2. Blanchard, Julian. The History of Electrical Resonance. *Bell Syst. Tech. J.* **20** (1941).
3. Pendry, J. B., Holden, A. J., Stewart, W. J. & Youngs, I. Extremely Low Frequency Plasmons in Metallic Mesostuctures. *Phys. Rev. Lett.* **76**, 4773–4776 (1996).
4. Shelby, R. A. Experimental Verification of a Negative Index of Refraction. *Science* **292**, 77–79 (2001).
5. Pendry, J. B. Negative Refraction Makes a Perfect Lens. *Phys. Rev. Lett.* **85**, 3966–3969 (2000).
6. Pendry, J. B. Controlling Electromagnetic Fields. *Science* **312**, 1780–1782 (2006).
7. Boyvat, M. & Hafner, C. V. Molding the flow of magnetic field with metamaterials: magnetic field shielding. *Prog. Electromagn. Res.* **126**, 303–316 (2012).
8. Boyvat, M. & Hafner, C. V. Magnetic Field Shielding by Metamaterials. *Prog. Electromagn. Res.* **136**, 647–664 (2013).
9. Kurs, A. *et al.* Wireless Power Transfer via Strongly Coupled Magnetic Resonances. *Science* **317**, 83–86 (2007).
10. Eichenfield, M., Michael, C. P., Perahia, R. & Painter, O. Actuation of micro-optomechanical systems via cavity-enhanced optical dipole forces. *Nat. Photonics* **1**, 416–422 (2007).
11. Rosenberg, J., Lin, Q. & Painter, O. Static and dynamic wavelength routing via the gradient optical force. *Nat. Photonics* **3**, 478–483 (2009).
12. Wiederhecker, G. S., Chen, L., Gondarenko, A. & Lipson, M. Controlling photonic structures using optical forces. *Nature* **462**, 633–636 (2009).
13. Wiederhecker, G. S., Manipatruni, S., Lee, S. & Lipson, M. Broadband tuning of optomechanical cavities. *Opt. Express* **19**, 2782–2790 (2011).
14. Lapine, M., Shadrivov, I. V., Powell, D. A. & Kivshar, Y. S. Metamaterials with conformational nonlinearity. *Sci. Rep.* **1** (2011).
15. Zhao, R., Tassin, P., Koschny, T. & Soukoulis, C. M. Optical forces in nanowire pairs and metamaterials. *Opt. Express* **18**, 25665–25676 (2010).
16. Lapine, M., Shadrivov, I. V., Powell, D. A. & Kivshar, Y. S. Magnetoelastic metamaterials. *Nat. Mater.* **11**, 30–33 (2012).
17. Liu, M., Powell, D. A. & Shadrivov, I. V. Chiral meta-atoms rotated by light. *Appl. Phys. Lett.* **101**, 031105 (2012).
18. Tang, C., Wang, Q., Liu, F., Chen, Z. & Wang, Z. Optical forces in twisted split-ring-resonator dimer stereometamaterials. *Opt. Express* **21**, 11783–11793 (2013).
19. Liu, M. *et al.* Nonlinear response via intrinsic rotation in metamaterials. *Phys. Rev. B* **87**, 235126 (2013).

20. Urzhumov, Y., Chen, W., Bingham, C., Padilla, W. & Smith, D. R. Magnetic levitation of metamaterial bodies enhanced with magnetostatic surface resonances. *Phys. Rev. B* **85**, 054430 (2012).
21. Liu, M., Powell, D. A., Shadrivov, I. V., Lapine, M. & Kivshar, Y. S. Self-oscillations in nonlinear torsional metamaterials. *New J. Phys.* **15**, 073036 (2013).
22. Sudo, S., Segawa, S. & Honda, T. Magnetic Swimming Mechanism in a Viscous Liquid. *J. Intell. Mater. Syst. Struct.* **17**, 729–736 (2006).
23. Yesin, K. B., Vollmers, K. & Nelson, B. J. Modeling and Control of Untethered Biomicrobots in a Fluidic Environment Using Electromagnetic Fields. *Int. J. Robot. Res.* **25**, 527–536 (2006).
24. Vollmers, K., Frutiger, D. R., Kratochvil, B. E. & Nelson, B. J. Wireless resonant magnetic microactuator for untethered mobile microrobots. *Appl. Phys. Lett.* **92**, 144103 (2008).
25. Abbott, J. J. *et al.* How Should Microrobots Swim? *Int. J. Robot. Res.* **28**, 1434–1447 (2009).
26. Frutiger, D. R., Vollmers, K., Kratochvil, B. E. & Nelson, B. J. Small, Fast, and Under Control: Wireless Resonant Magnetic Micro-agents. *Int. J. Robot. Res.* **29**, 613–636 (2010).
27. Nelson, B. J., Kaliakatsos, I. K. & Abbott, J. J. Microrobots for Minimally Invasive Medicine. *Annu. Rev. Biomed. Eng.* **12**, 55–85 (2010).
28. Steager, E. B. *et al.* Automated biomanipulation of single cells using magnetic microrobots. *Int. J. Robot. Res.* **32**, 346–359 (2013).
29. Fusco, S. *et al.* Targeted Delivery: An Integrated Microrobotic Platform for On-Demand, Targeted Therapeutic Interventions (Adv. Mater. 6/2014). *Adv. Mater.* **26**, 951–951 (2014).
30. Agarwal, A. K., Sridharamurthy, S. S., Beebe, D. J. & Jiang, H. Programmable autonomous micromixers and micropumps. *J. Microelectromechanical Syst.* **14**, 1409–1421 (2005).
31. Sershen, S. R. *et al.* Independent Optical Control of Microfluidic Valves Formed from Optomechanically Responsive Nanocomposite Hydrogels. *Adv. Mater.* **17**, 1366–1368 (2005).
32. Donald, B. R., Levey, C. G. & Paprotny, I. Planar Microassembly by Parallel Actuation of MEMS Microrobots. *J. Microelectromechanical Syst.* **17**, 789–808 (2008).
33. Sitti, M. Miniature devices: Voyage of the microrobots. *Nature* **458**, 1121–1122 (2009).
34. Floyd, S., Diller, E., Pawashe, C. & Sitti, M. Control methodologies for a heterogeneous group of untethered magnetic micro-robots. *Int. J. Robot. Res.* **30**, 1553–1565 (2011).
35. Diller, E., Miyashita, S. & Sitti, M. Remotely addressable magnetic composite micropumps. *RSC Adv.* **2**, 3850–3856 (2012).
36. Diller, E., Giltinan, J. & Sitti, M. Independent control of multiple magnetic microrobots in three dimensions. *Int. J. Robot. Res.* **32**, 614–631 (2013).
37. Donald, B. R., Levey, C. G., Paprotny, I. & Rus, D. Planning and control for microassembly of structures composed of stress-engineered MEMS microrobots. *Int. J. Robot. Res.* **32**, 218–246 (2013).
38. Cornelissen, S. A., Hartzell, A. L., Stewart, J. B., Bifano, T. G. & Bierden, P. A. MEMS deformable mirrors for astronomical adaptive optics. in *SPIE Astron. Telesc. Instrum. Obs. Front. Astron. New Decade 7736*, 77362D–77362D–10 (International Society for Optics and Photonics, 2010).
39. Gavel, D. T. Progress update on the visible light laser guidestar experiments at Lick Observatory. in *MOEMS-MEMS 7595*, 759508–759508–6 (International Society for Optics and Photonics, 2010).
40. Gavel, D. *et al.* Visible light laser guidestar experimental system (Villages): on-sky tests of new technologies for visible wavelength all-sky coverage adaptive optics systems. in *Proc SPIE 7015*, 70150G–70150G–11 (2008).
41. Liu, A. Q., Zhu, W. M., Tsai, D. P. & Zheludev, N. I. Micromachined tunable metamaterials: a review. *J. Opt.* **14**, 114009 (2012).
42. Ou, J. Y., Plum, E., Jiang, L. & Zheludev, N. I. Reconfigurable Photonic Metamaterials. *Nano Lett.* **11**, 2142–2144 (2011).
43. Capanu, M., Boyd, J. G. I. & Hesketh, P. J. Design, fabrication, and testing of a bistable electromagnetically actuated microvalve. *J. Microelectromechanical Syst.* **9**, 181–189 (2000).
44. Lu, L.-H., Ryu, K. S. & Liu, C. A magnetic microstirrer and array for microfluidic mixing. *J. Microelectromechanical Syst.* **11**, 462–469 (2002).
45. Mensing, G. A., Pearce, T. M., Graham, M. D. & Beebe, D. J. An externally driven magnetic microstirrer. *Philos. Trans. R. Soc. Lond. Ser. Math. Phys. Eng. Sci.* **362**, 1059–1068 (2004).
46. Lee, S.-W., Kim, J.-D., Son, J.-H., Ryu, M.-H. & Kim, J. Design of Two-Dimensional Coils for Wireless Power Transmission to In Vivo Robotic Capsule. in *Eng. Med. Biol. Soc. 2005 IEEE-EMBS 2005 27th Annu. Int. Conf. Of 6631–6634* (2005). doi:10.1109/IEMBS.2005.1616022.
47. Lenaerts, B. & Puers, R. Inductive powering of a freely moving system. *Eurosensors XVIII 2004 18th Eur. Conf. Solid-State Transducers* **123–124**, 522–530 (2005).
48. Lenaerts, B. & Puers, R. An inductive power link for a wireless endoscope. *Biosens. Bioelectron.* **22**, 1390–1395 (2007).
49. Xin, W., Yan, G. & Wang, W. Study of a wireless power transmission system for an active capsule endoscope. *Int. J. Med. Robot.* **6**, 113–122 (2010).
50. Jackson, J. D. *Classical electrodynamics*. (Wiley, 1975).
51. Shamonina, E. & Solymar, L. Diamagnetic properties of metamaterials: a magnetostatic analogy. *Eur. Phys. J. B* **41**, 307–312 (2004).
52. Balanis, C. A. *Antenna theory: analysis and design*. (Wiley Interscience, 2005).



53. Tretyakov, S. *Analytical Modeling in Applied Electromagnetics*. (Artech House, 2003).
54. Smythe, W. R. *Static and Dynamic Electricity*. (McGraw-Hill, 1950).

## Acknowledgments

We thank Prof. Bradley Nelson and his group, especially Dr. Mahmut Selman Sakar for useful discussions; Claudio Maccio for mechanical design and manufacturing; EWZ Zurich for financial support.

## Author contributions

M.B. performed the computations, experiments and prepared the manuscript. C.H. proposed the asymmetric motor concept. C.H. and J.L. directed the project and revised the manuscript. All the authors intensively discussed various aspects.

## Additional information

**Supplementary information** accompanies this paper at <http://www.nature.com/scientificreports>

**Competing financial interests:** The authors declare no competing financial interests.

**How to cite this article:** Boyvat, M., Hafner, C. & Leuthold, J. Wireless control and selection of forces and torques - towards wireless engines. *Sci. Rep.* 4, 5681; DOI:10.1038/srep05681 (2014).



This work is licensed under a Creative Commons Attribution-NonCommercial-NoDerivs 4.0 International License. The images or other third party material in this article are included in the article's Creative Commons license, unless indicated otherwise in the credit line; if the material is not included under the Creative Commons license, users will need to obtain permission from the license holder in order to reproduce the material. To view a copy of this license, visit <http://creativecommons.org/licenses/by-nc-nd/4.0/>